Universal plasmonic properties of two-dimensional nanoparticles possessing sharp corners

B. Sturman,[1] E. Podivilov,[1] and M. Gorkunov[2]
[1]*Institute of Automation and Electrometry, Russian Academy of Sciences, 630090 Novosibirsk, Russia*
[2]*Shubnikov Institute of Crystallography, Russian Academy of Sciences, 119333 Moscow, Russia*
(Received 24 July 2012; published 7 March 2013)

We investigate theoretically the impact of variable smoothing of corners of single metallic, two-dimensional nanoparticles (faceted nanowires) on the characteristics of their plasmonic resonances—the resonant frequencies, eigenfunctions, polarizability, and near fields—using the method of surface integral equations. This impact is very strong: Increasing sharpness of the corners leads to a strong separation of the plasmonic eigenfrequencies, a progressing localization of the surface charge at the corners, and a strong near-field enhancement of the light intensity. Dependences of the above characteristics on the apex angle and the corner curvature show striking universal features. The limit of nonsmoothed corners is found to be practically meaningless.

DOI: 10.1103/PhysRevB.87.115406 PACS number(s): 73.20.Mf, 42.25.Fx, 78.40.Kc

I. INTRODUCTION

Plasmon excitations of subwavelength (nanosize) metallic particles, including two-dimensional (2D) particles (nanowires), is nowadays a vast and rapidly developing research area. Potential applications of nanoplasmons span from nanolasers[1–3] (spasers) to biosensors and sensors of single atoms and molecules.[4,5] From a fundamental point of view, it is interesting and important to recognize the capabilities of tailoring the plasmonic resonances and the extents of concentration of light energy within the nanoscale.

Strong enhancement of the light fields near sharp features of the metal-dielectric interfaces—corners and tips—is well known in electrodynamics as the so-called corner singularities.[6–8] These singularities are important in the theory of composites, when the inclusions possess sharp surface features.[9–11] In the case of metal, whose optical dielectric permittivity $\varepsilon_{\mathrm{M}} = \varepsilon'_{\mathrm{M}} + i\varepsilon''_{\mathrm{M}}$ has a negative real part $\varepsilon'_{\mathrm{M}}$, the singular behavior acquires special features: Depending on the apex angle of a single 2D corner, there are two negative critical values of ε_{M} leading to diverging light energy.[7,8] These critical values are, e.g., $-1/3$ and -3 for a 90° single corner. They manifest themselves also in the properties of the so-called wedge plasmons propagating along sharp corners.[12,13]

In theory, the presence of sharp surface features is often regarded as something nonphysical and leading to divergence of numerical procedures for finite-size metal-dielectric structures—rounding of sharp corners is a standard element of numerical methods.[14] Moreover, the mathematical basis of the plasmonic theory, including the well-known potential theory, is restricted to sufficiently smooth (Lyapunov) surfaces, i.e., surfaces possessing no cusps.[15–17] Only recently, a serious mathematical attempt has been made to overcome this restriction.[18]

From the experimental point of view, the presence of sharp corners and tips in metallic 2D and 3D nanoparticles is a feature which is far from exotic. Modern chemical methods for the production of such particles give often nearly atomically sharp edges in the crystallographic directions.[19–21] In particular, the synthesis of metallic nanostars has recently allowed a strong enhancement of the near fields at the plasmonic resonances.[22] Experimental methods capable of resolving, spectrally and spatially, plasmonic excitations of faceted nanoparticles are emerging nowadays.[23]

Analytical solutions to Maxwell's equations relevant to the plasmonic eigenmodes of metallic 2D and 3D single nanoparticles are available only in the simplest cases—circular and elliptic cylinders, spheres, and ellipsoids; see, e.g., Refs. 24 and 25, and references therein. They give strongly degenerated plasmonic resonances. In particular, all plasmonic excitations of a circular cylinder correspond to a single eigenfrequency given by $\varepsilon'_{\mathrm{M}}(\omega) = -1$.

Using different direct numerical methods, serious efforts have been undertaken to ascertain the phenomenology of the optical response of 2D and 3D metallic nanoparticles of more complicated shapes.[26–31] In particular, truncated cubes and polyhedrons, snipped triangular prisms, and wires with nonregular cross sections were considered. The general outcome is that the deviations from the most symmetric shapes result in enriching plasmon spectrum and in the appearance of new red-shifted resonances. The expected near-field enhancement of the light intensity near the corners was also demonstrated. For 2D nanoparticles, the strongest shape effects were found for a triangular cross section.

An important step in the theory of plasmonic resonances of nanoparticles possessing Lyapunov boundaries was made in Refs. 32 and 33. Using the quasistatic approximation[25] and the theory of potential,[17] it was shown that the plasmonic eigenfrequencies and eigenfunctions can be found by solving a basic integral equation for surface-charge density at the boundary of the nanoparticle. The knowledge of these basic ingredients allows one to next determine such important characteristics as the width of the plasmonic resonance, polarizability of the particle, and near fields using a simple perturbation routine.[15,33] Size corrections to the quasistatic characteristics are also available.[15,34]

The approach of Refs. 32 and 33 possesses highly attractive features as applied to the case of nanoparticles whose characteristic size r_0 is small compared to the wavelength λ: In the leading approximation in r_0/λ, the resonant plasmonic frequencies are size invariant—they are determined by the shape of the particle, while the plasmonic eigenfunctions are scaling invariant.[35] The determination of the resonant values of the permittivity, denoted as ε, is free of model assumptions

about the frequency dispersion of this quantity. In short, the plasmonic excitations of metallic nanoparticles can be viewed as a geometric issue. The reduction of the dimension of the problem to be solved is also important. It increases the capability and accuracy of numerical methods and allows one to consider very sharp tips and corners of metallic particles.

Below we analyze the impact of a variable smoothing of corners of 2D nanoparticles, possessing different shapes and apex angles, on the plasmonic spectrum, the modal charge distributions, the polarizability, and the near-field enhancement. Our considerations show that for large values of the normalized corner curvature κ_c, i.e., the ratio of the size r_0 to the corner curvature radius ρ_c, plasmonic properties acquire a *universal behavior*: The lowest resonant values of ε (dipolar and multipolar) are controlled by κ_s and by the apex angle θ_a, while the global shape is of minor importance. Moreover, the lowest values of ε tend to $1 - 2\pi\theta_a^{-1}$ with increasing κ_c and become well separated from the higher values.

The universality of the plasmonic behavior manifests itself also in a progressive localization of the modal charge at the corners of nanoparticles with increasing κ_c. We analyze this phenomenon in detail proceeding from the case of circular symmetry to the cases of weak fourfold rotational symmetry and further on to the cases of arbitrary-sharp smoothing of 90° corners of a square. Altogether, strong lowering of the resonant values of ε and localization of the corresponding eigenfunctions enable one to excite the corresponding dipolar branches selectively, leading to a dramatic near-field enhancement of the incident light.

II. BASIC RELATIONS

The optical properties of subwavelength particles, including the plasmonic properties of metallic nanoparticles, can be well described on the basis of the quasistatic approximation.[25] In the leading approximation, the amplitude of the electric light field at the frequency ω can be expressed as $\mathbf{E} = -\nabla\phi$, and the potential ϕ obeys the Laplace equation inside and outside the particle and satisfies the conventional boundary conditions incorporating the optical permittivity of the particle $\varepsilon_{\mathrm{M}} = \varepsilon_{\mathrm{M}}(\omega)$. Two steps have to be taken as applied to plasmonic resonances of nanoparticles:

(i) First, it is necessary to solve an eigenmode problem to determine the real resonant values of the optical permittivity ε and the corresponding plasmonic eigenfunctions, ignoring the light absorption. The most elegant and efficient formulation of the eigenmode problem occurs in the terms of the eigenmode surface-charge density σ at the border of the metallic particle.

(ii) Second, one can describe the optical properties of the nanoparticle subjected to an external light field in the eigenmode problem terms.

As applied to the 2D case, the plasmonic eigenmode problem is reduced to the solution of a real 2D integral equation for the surface-charge density $\sigma(\mathbf{r})$,[32,33]

$$\int_L K(\mathbf{r},\mathbf{r}')\,\sigma(\mathbf{r}')\,dl' = \Lambda\,\sigma(\mathbf{r}), \quad \mathbf{r},\mathbf{r}' \in L, \tag{1}$$

where the closed line L is the boundary of the particle, dl is the length element along L, $\Lambda = (\varepsilon+1)/(\varepsilon-1)$ is the eigenvalue to be found, and the kernel is given by

$$K(\mathbf{r},\mathbf{r}') = \frac{\mathbf{n}\cdot(\mathbf{r}-\mathbf{r}')}{\pi\,(\mathbf{r}-\mathbf{r}')^2}, \tag{2}$$

with $\mathbf{n} = \mathbf{n}(\mathbf{r})$ being the unit vector of the external normal. It is assumed that the line L is smooth—having no cusps. In this case, a 0/0 uncertainty in $K(\mathbf{r},\mathbf{r}')$ for $\mathbf{r} \to \mathbf{r}'$ can be resolved.

Generally, Eq. (1) gives an infinite discrete sequence of the plasmonic eigenmodes. When necessary, we will use the notation ε_j, Λ_j, $\sigma_j(\mathbf{r})$, ..., with the subscript j enumerating these modes. This subscript should not necessarily be an integer.

Equations (1) and (2) possess a number of simple and general properties:[32,33]

(a) If the $\mathbf{r}$, $\mathbf{r}'$ belong to a plane section of L, then $K(\mathbf{r},\mathbf{r}') = 0$.

(b) The kernel is not symmetric, $K(\mathbf{r},\mathbf{r}') \neq K(\mathbf{r}',\mathbf{r})$, i.e., the eigenmode problem is not Hermitian.

(c) All eigenvalues ε are real and negative.

(d) The total surface charge is zero, $\int_L \sigma(\mathbf{r})\,dl = 0$.

(e) For any L, there is an eigenvalue $\Lambda = 0$, i.e., $\varepsilon = -1$.

(f) If L is a circle of a radius r_0, then $K(\mathbf{r},\mathbf{r}') = 1/2\pi r_0$ and $\varepsilon = -1$, i.e., total degeneracy of the eigenvalues occurs.

(g) If r_0 is a size parameter, then the eigenvalues are r_0 independent, while the eigenfunctions σ depend on $\mathbf{r}/r_0$, i.e., they are scale invariant.

The following important general properties are less evident:[33]

(a) If ε is an eigenvalue, then the inverse $1/\varepsilon$ is an eigenvalue as well. This is the property of twin symmetry inherent in the 2D case.

(b) Since the eigenmode problem is not Hermitian, different eigenfunctions are not orthogonal, $\int_L \sigma_{j_1}(\mathbf{r})\,\sigma_{j_2}(\mathbf{r})\,dl \neq 0$ for $j_1 \neq j_2$.

(c) For this reason, it is necessary to employ not only the eigenfunctions $\sigma(\mathbf{r})$, but also the eigenfunctions $\tau(\mathbf{r})$ of the adjoint problem

$$\int_L K(\mathbf{r}',\mathbf{r})\,\tau(\mathbf{r}')\,dl' = \Lambda\,\tau(\mathbf{r}), \tag{3}$$

corresponding to the transposed kernel and the same eigenvalue Λ.

(d) The adjoint eigenfunctions allow us to employ the orthogonality relations $\langle\sigma_{j_1}(\mathbf{r})\,\tau_{j_2}(\mathbf{r})\rangle = 0$, where $j_1 \neq j_2$ and $\langle\cdot\rangle$ means the integration along L.

Despite the simplifying general properties, the eigenmode problem is far from trivial. Further simplifications are possible with the use of properties of spatial symmetry.[36] In particular, depending on the spatial symmetry of the nanoparticle, an eigenmode j can possess zero or nonzero modal dipole moment $\mathbf{d}_j = \langle\mathbf{r}\sigma_j(\mathbf{r})\rangle$. The dipolar eigenmodes are of our prime interest.

As soon as the eigenmode problem is solved, the calculation of the optical characteristics of the nanoparticle can be done straightforwardly. Let the total electric light field be $\mathbf{E} = \mathbf{E}_0 + \hat{\mathbf{E}}(\mathbf{r})$, where $\mathbf{E}_0$ is the amplitude of a locally uniform external light field which is present without the particle and $\hat{\mathbf{E}}(\mathbf{r})$ is the nonuniform particle-caused part to be found. Just this nonuniform part will be represented by the light-induced surface-charge density $\hat{\sigma}$. Here and later on, we use the hat

symbol in order to distinguish the light-induced charge density from the density σ_j (or σ) related to the eigenmodes.

Generally, the density $\hat{\sigma}(\mathbf{r})$ is given by the modal expansion

$$\hat{\sigma}(\mathbf{r}) = \sum_j c_j \, \sigma_j(\mathbf{r}). \tag{4}$$

The calculation of the constants c_j consists of three steps:[33]

(i) First, we employ the known relation of the potential theory for the normal component of the total field E_n on the external $(+)$ and the internal $(-)$ sides of the line L:

$$E_n^{\pm} = \mathbf{E}_0 \cdot \mathbf{n} \pm 2\pi\hat{\sigma}(\mathbf{r}) + \int_L 2\hat{\sigma}(\mathbf{r}') \, \frac{\mathbf{n} \cdot (\mathbf{r} - \mathbf{r}')}{|\mathbf{r} - \mathbf{r}'|^2} \, d\mathbf{r}'. \tag{5}$$

Each of the three contributions is intuitively clear.

(ii) Second, we use the boundary condition $E_n^+ = \varepsilon_{\mathrm{M}} E_n^-$. Combining it with Eq. (5), we get

$$(\mathbf{E}_0 \cdot \mathbf{n})/2\pi = \tilde{\Lambda}\,\hat{\sigma}(\mathbf{r}) - \int_L K(\mathbf{r},\mathbf{r}')\,\hat{\sigma}(\mathbf{r}')\,d\mathbf{r}', \tag{6}$$

with $\tilde{\Lambda} = (\varepsilon_{\mathrm{M}} + 1)/(\varepsilon_{\mathrm{M}} - 1)$.

(iii) Third, using Eq. (4) and the orthogonality relations between the eigenfunctions $\tau_{j_1}(\mathbf{r})$ and $\sigma_{j_2}(\mathbf{r})$, we obtain

$$c_j = \frac{(\varepsilon_{\mathrm{M}} - 1)(\varepsilon_j - 1)}{\varepsilon_j - \varepsilon_{\mathrm{M}}} \frac{\langle \tau_j (\mathbf{E}_0 \cdot \mathbf{n})\rangle}{4\pi \, \langle \tau_j \sigma_j \rangle}. \tag{7}$$

The complex-valued factor $\varepsilon_j - \varepsilon_{\mathrm{M}}(\omega)$ in the denominator reaches the minimum absolute values $|\varepsilon''_{\mathrm{M}}(\omega_j)|$ at the points of plasmonic resonances, such that $\varepsilon'_{\mathrm{M}}(\omega_j) = \varepsilon_j$. If needed, the radiation losses can be taken into account in Eq. (7) in addition to the joule losses caused be the imaginary part of the permittivity $\varepsilon''_{\mathrm{M}}$.

If $\varepsilon_{\mathrm{M}}(\omega) \simeq \varepsilon_j$, then we can keep only one resonant term in the expansion (4) and obtain, for the light-induced surface-charge density,

$$\hat{\sigma}_j(\mathbf{r}) \simeq \frac{(\varepsilon_j - 1)^2}{(\varepsilon_j - \varepsilon_{\mathrm{M}})} \times \frac{\langle \tau_j \, (\mathbf{E}_0 \cdot \mathbf{n})\rangle}{4\pi \, \langle \tau_j \sigma_j \rangle} \, \sigma_j(\mathbf{r}). \tag{8}$$

The first factor is resonant in ω and the second one expresses the spatial properties of the eigenfunctions. Importantly, the found relation does not depend on the normalization of the eigenfunctions $\sigma_j(\mathbf{r})$ and $\tau_j(\mathbf{r})$.

With the light-induced surface density $\hat{\sigma}(\mathbf{r})$ known, we can calculate the dipole moment of the particle, $\mathbf{d} = \langle \mathbf{r}\,\hat{\sigma}(\mathbf{r})\rangle$, its polarizability, irradiated power, etc.

III. PARAMETRIZATION OF THE SHAPE

In the 2D case, the polar coordinate system, $\mathbf{r} = (x,y) = (r\cos\varphi, r\sin\varphi)$ with $r = r(\varphi)$ and the origin inside L, provides a natural choice of a single-variable coordinate along L, namely, the polar angle φ. Any 2π-periodic function $r(\varphi)$ specifies L. Three geometric characteristics of this boundary line are of interest to us:

(i) First, this is the derivative $l_\varphi = dl/d\varphi$. It is given by $l_\varphi = (r^2 + r_\varphi^2)^{1/2}$, where $r_\varphi = dr/d\varphi$. From now on, the subscript φ indicates the polar angle derivative.

(ii) Second, this is the unit vector of the external normal $\mathbf{n} = (r_\varphi \sin\varphi + r\cos\varphi, -r_\varphi\cos\varphi + r\sin\varphi)/l_\varphi$.

(iii) Third, this is the local curvature radius $\rho = l_\varphi^3/(r^2 + 2r_\varphi^2 - r r_{\varphi\varphi})$.

In the polar coordinates, it is practical to transfer from the linear charge density $\sigma(\mathbf{r})$ to the angular density $\sigma(\varphi) = \sigma[\mathbf{r}(\varphi)]\,dl/d\varphi$, such that the surface-charge differential is $\sigma(\varphi)d\varphi$. Using the above relations, we rewrite Eq. (1) in the form

$$\int_0^{2\pi} K(\varphi,\varphi')\,\sigma(\varphi')\,d\varphi' = \Lambda\,\sigma(\varphi), \tag{9}$$

with the kernel

$$K(\varphi,\varphi') = \frac{r^2 - rr'\cos(\varphi - \varphi') - r_\varphi r'\sin(\varphi - \varphi')}{\pi\,[r^2 + r'^2 - 2rr'\cos(\varphi - \varphi')]}. \tag{10}$$

Only the last term in the numerator makes the kernel not symmetric in φ and φ'. In the case of circle $r(\varphi) = \mathrm{const}$, we have $K(\varphi,\varphi') = 1/2\pi$. Resolving a $0/0$ uncertainty in Eq. (10) for $\varphi' \to \varphi$, we obtain, for the diagonal value of the kernel, $K(\varphi,\varphi) = l_\varphi/2\rho$; this gives a link to the geometric characteristics of L. It is evident that $K(\varphi,\varphi)$ peaks at the points of minimum of $\rho(\varphi)$.

It is easy to find that the integral equation for the adjoint function $\tau(\mathbf{r})$ is different from Eq. (9) for $\sigma(\varphi)$ only by the replacement $K(\varphi,\varphi') \to K(\varphi',\varphi)$.

Below, we use two basic families of lines L. The first family (two-parametric one) is given by the relation

$$\frac{r}{r_0} = \frac{p+1}{\sqrt{c^2 + p^2 s^2 \cot^2(\theta_a/2)} + \sqrt{s^2\cot^2(\theta_a/2) + p^2 c^2}}, \tag{11}$$

where $c = \cos\varphi$ and $s = \sin\varphi$, while p and θ_a are two parameters ranging within the intervals $[1,\infty]$ and $[0,\pi/2]$, respectively. The maximum value of $r(\varphi)$ is r_0; it corresponds to $\varphi = 0$ and π. For $p \gg 1$, the line L is a smoothed rhombus with the sharp apex angle θ_a, while for $p \to 1$, it transfers into an ellipse with the axes ratio $\cot\theta_a$; see also Fig. 1(a).

For $\theta_a = \pi/2$, we have a smoothed square transferring into a circle of the radius r_0 with decreasing p. The normalized corner curvature is given by $\kappa_c = r_0/\rho_c = \cot^2(\theta_a/2)(p - 1 + p^{-1})$; it is practically linear in p for $p \gg 1$. Thus, the limit $p \to \infty$ corresponds to a perfect rhombus. Note that for $p \gg 1$, the line L is very close to the perfect rhombus everywhere except close vicinities of the corners.

The second family of lines (single-parametric one) is given by the relation

$$\frac{r}{r_0} = \frac{1 + 9b^2}{[f(\varphi) + f(\varphi - 2\pi/3) + f(\varphi + 2\pi/3)]^2 - 2}, \tag{12}$$

with $f(\varphi) = [\sin^2(\varphi/2) + b^2]^{1/2}$ and $0 < b < \infty$. The structure of Eq. (12) ensures the $3m$ symmetry of L. For $b \gg 1$, line L is very close to a r_0 circle. With decreasing b, it

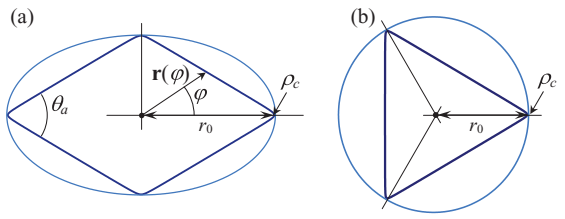

FIG. 1. (Color online) (a) The boundary line L for a smoothed rhombus ($\theta_a = \pi/3$, $p = 50$) transferring to an ellipse. (b) A smoothed equilateral triangle ($b = 0.01$) transferring to a circle.

transforms into a smoothed equilateral triangle corresponding to $\theta_a = \pi/3$; see also Fig. 1(b). For $b \ll 1$, the normalized corner curvature is $\kappa_c \simeq \sqrt{3}/2b$; it tends to ∞ for $b \to 0$.

Parametrizations of Eqs. (11) and (12) are not unique. In particular, we will use an additional q representation of L given by

$$r/r_0 = (|c|^{2q} + |s|^{2q})^{-1/2q}, \tag{13}$$

with $0 \leqslant q < \infty$. It gives a smoothed square for $q \gg 1$ transferring into a r_0 circle for $q \to 1$. At the same value of κ_c, line L lies here inside that given by Eq. (11) with $\theta_a = \pi/2$. The q representation is useful to verify whether the plasmonic properties are controlled by the corner curvature for $\kappa_c \gg 1$ at the same values of θ_a.

IV. SYMMETRY CONSIDERATIONS

The presence of point symmetry of the cross section allows one to classify the plasmonic eigenfunctions and eigenvalues and to simplify numerical calculations regardless of the smoothing details.[36] For illustration, we consider here the case of the highest point symmetry $4m$, which is inherent in square-shaped 2D particles. In this case, there are doubly degenerate dipolar modes and four types of nondegenerate multipolar modes.

One of two dipolar $[d]$ eigenfunctions belonging to an eigenvalue ε obeys the symmetry requirements

$$\sigma(\varphi) = \sigma(-\varphi) = -\sigma(\pi - \varphi); \quad [d]\,. \tag{14}$$

They mean that $\sigma(\mathbf{r})$ is symmetric about the horizontal (h) diagonal and antisymmetric about the vertical (v) diagonal; see also Figs. 1(a) and 2. The dipole moment is directed here along the h diagonal, and $\sigma(\pm\pi/2) = 0$.

Using the symmetry relations (14), we find that

$$\int_0^{2\pi} K(\varphi,\varphi')\sigma(\varphi')\,d\varphi' = \int_0^{\pi/2} K_d(\varphi,\varphi')\sigma(\varphi')\,d\varphi', \tag{15}$$

where the dipolar kernel $K_d(\varphi,\varphi')$ is given by

$$K_d = K(\varphi,\varphi') + K(\varphi,-\varphi') - K(\varphi,\pi-\varphi') - K(\varphi,\pi+\varphi').$$

It is possible thus to solve the eigenmode problem for the dipolar modes within the interval $[0,\pi/2]$; this interval is sufficient to restore $\sigma(\varphi)$ in the whole angular range. The function $K_d(\varphi,\varphi')$ is smooth and sign changing, but not trivial. Note that $K_d(\pi/2,\varphi') = 0$; this is consistent with the equality $\sigma(\pm\pi/2) = 0$.

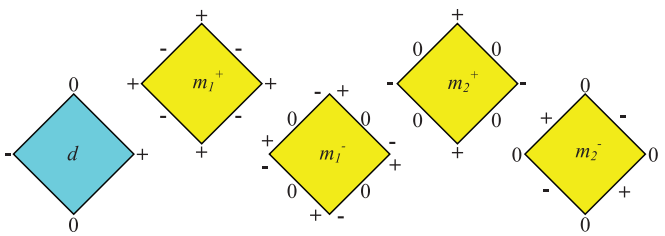

FIG. 2. (Color online) Possible types of the dipolar (d) and multipolar ($m^{\pm}_{1,2}$) symmetry. Inversion of the charge signs does not change the symmetry.

The second independent dipolar eigenfunction, belonging to the same eigenvalue ε and not shown in Fig. 2, can be obtained by a trivial $\pi/2$ rotation. It is given by $\sigma(\varphi - \pi/2)$, and the corresponding dipole moment is directed along the v diagonal. Moreover, one can show that the dipolar eigenfunctions are orthogonal to each other.

The same reduction procedure is valid for the determination of the adjoint dipolar eigenfunctions $\tau(\varphi)$. The choice of independent dipolar eigenfunctions is not unique. Taking, e.g., the combinations $\sigma(\varphi) \pm \sigma(\varphi - \pi/2)$, one obtains the eigenfunctions whose dipole moments are $\pi/4$ rotated against the initial ones.

All multipolar $[m]$ modes are nondegenerate in ε and inversion symmetric, $\sigma(\varphi) = \sigma(\varphi \pm \pi)$. Generally, there are four types of the multipolar symmetry (see also Fig. 2):

$$\sigma(\varphi) = \sigma(\varphi + \pi/2) = \pm\sigma(-\varphi); \quad [m_1^{\pm}], \tag{16a}$$

$$\sigma(\varphi) = -\sigma(\varphi + \pi/2) = \pm\sigma(-\varphi); \quad [m_2^{\pm}], \tag{16b}$$

(i) The first type, m_1^+: Symmetry to all allowed symmetry transformations—rotations and reflections.

(ii) The second type, m_1^-: Symmetry to all allowed rotations and asymmetry to all allowed reflections.

(iii) The third type, m_2^+: Symmetry to the reflections about the diagonals, but asymmetry to the $\pi/2$ rotations and to the reflections about the lines passing through the centers of the opposite sides.

(iv) The fourth type, m_2^-: Asymmetry to the $\pi/2$ rotations and to the reflections about the diagonals, but symmetry to the reflections about the lines passing through the centers of the opposite sides.

It is not difficult to write down two separate integral equations within the interval $[0,\pi/2]$ for the multipolar symmetry types $m_1^{\pm}$ and $m_2^{\pm}$.

Employment of the integral equations for the special types of symmetry resolves the problem of classification of the eigenmodes and, furthermore, extends the capabilities of numerical calculations for very small corner curvatures; see the next section. It is necessary, of course, to make sure that the found particular solutions exhaust the solutions of the general integral equation (9).

V. NUMERICAL RESULTS

We solved numerically the general integral equation (1) for $\sigma(\varphi)$ and the transposed equation for $\tau(\varphi)$. Also, we solved the integral equations for the particular types of symmetry within the reduced angular interval $[0,\pi/2]$. It was verified for not very high values of corner curvature parameter $\kappa_c = r_0/\rho_c$ that the reduced equations provide full information about the eigenfunctions and eigenvalues. For ultimately small corner curvature parameter, $\kappa_c \gtrsim 10^4$, we used the reduced integral equations.

The number of points N per side varied from 201 to 1001. In order to enter the range of high κ_c, we used nonuniform discretizations with the density of points near the corners $\sim N^3$. For any particular value of the parameters p, b, and q [see Eqs. (11), (12), and below], it was ensured that further increase of N does not affect $\varepsilon(p)$, $\varepsilon(b)$, and $\varepsilon(q)$.

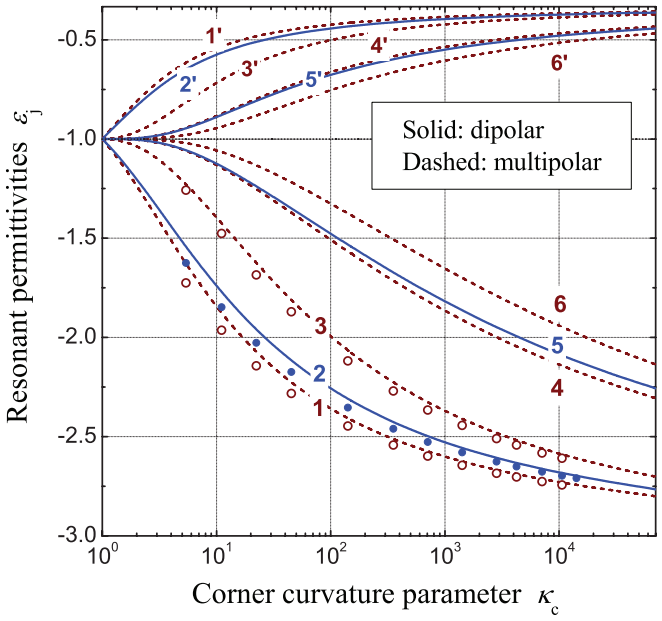

FIG. 3. (Color online) The case of square, $\theta_a = \pi/2$. Dependence $\varepsilon(\kappa_c)$ for several first pairs of the plasmonic modes j, j'. Line L given by Eqs. (11) and (13) (lines and circles, respectively). The solid lines and filled circles refer to the dipolar modes, and the dashed lines and open circles represent the multipolar modes. For $j > 3$, the circles lie too close to the corresponding lines to be shown.

We show below that Eq. (11) with $\theta_a = \pi/2$ and Eq. (13) give essentially the same results for the eigenvalues and eigenfunctions of square for sufficiently large values of κ_c. With this fact proven, we restrict ourselves then to the representations given by Eqs. (11) and (12).

A. Spectra of eigenvalues

Consider first the case of square when the line L is given by Eq. (11) with $\theta_a = \pi/2$ and Eq. (13). Figure 3 shows our numerical results for the first several branches $\varepsilon_j(\kappa_c)$, possessing the largest distances to the value of -1, on a semilogarithmic scale. The eigenvalues appear in pairs j, j' linked by the twin symmetry: each value $\varepsilon_j < -1$ has its twin counterpart $\varepsilon_{j'} = 1/\varepsilon_j > -1$. The values of ε_j for the higher modes lie thus above line 6, and the close vicinity of the line $\varepsilon = -1$ is filled up with the spectrum. The main results, shown by lines, correspond to Eq. (11), while the circles refer to Eq. (13). The solid and dashed lines correspond to the dipolar and multipolar modes.

A number of further important features of the dependences $\varepsilon_j(\kappa_c)$ have to be indicated:

(a) All eigenvalues lie within the interval $[-1/3,3]$, restricted by the points of strong singularities for $\theta_a = \pi/2$,[7] and approach slowly the borders of this interval with increasing κ_c.

(b) Equations (11) and (13) give very close values of ε_j for $\kappa_c \gg 1$. The largest distances to -1 correspond to Eq. (13), i.e., to the fastest convergence to the perfect-square shape with increasing κ_c.

(c) The modes $1,2,3,4,\ldots$ possess the symmetries m_2^+, d, m_1^+, m_2^+, $\ldots$, respectively, whereas for the twin modes $1',2',3',4',\ldots$, the sequence of the symmetry changes is m_2^-, d, m_1^-, m_2^-, $\ldots$; see also Fig. 2.

(d) For $\kappa_c \gg 1$, the values of ε_j group in triplets. The *absolutely lowest* value ε_1 corresponds to the multipolar symmetry m_2^+, which is not the highest for the multipolar modes; see the next section.

(e) In the range $1 \leqslant \kappa_c \lesssim 10$, the changes of $\varepsilon_j(\kappa_c)$ occur linearly only for the first two pairs of branches, $1,1'$ and $2,2'$. This feature, valid also for the $3m$ symmetry, is in agreement with the theory of Ref. 37 developed for weak perturbations of the circular shape. The higher the mode number $j > 2$, the slower are the initial changes of $\varepsilon_j(\kappa_c)$.

(f) For $\kappa_c \gtrsim 10$, when the shape changes are already reduced to increasing sharpness of the corners, the decrease of $\varepsilon_j(\kappa_c)$ for the lowest modes still remains substantial.

(g) For $\kappa_c \gtrsim 10^3$, the branches $\varepsilon_{1,2}(\kappa_c)$ and $\varepsilon_{1',2'}(\kappa_c)$ approach the limiting values of -3 and $-1/3$ very slowly: for $\kappa_c > 10^4$, we are still pretty far from these values.

(h) Even for modest smoothing, $\kappa_c = 10^1$–10^2, the separation of the eigenvalues within the interval $[-3,-1]$ is big enough for their selective excitation.

Now we turn to the impact of the apex angle θ_a on the dependence $\varepsilon(\kappa_c)$. We consider the cases of rhombus with $\theta_a = \pi/2,\pi/3,\pi/4,\pi/5$, and $\pi/6$ using Eq. (11) and the case of an equilateral triangle using Eq. (12). For simplicity, we restrict ourselves to the lowest dipolar branch.

The corresponding data are presented in Fig. 4. The starting nonunit values of ε_1 coincide with the known plasmonic solutions for the elliptic cross section.[25] Obviously, a decrease of θ_a results in a strong lowering of the branches, including the initial and limiting values of $\varepsilon(\kappa_c)$. The limiting values, shown by the horizontal dashed lines, correspond to the general relation $\varepsilon(\infty) = 1 - 2\pi/\theta_a$ for nonintegrable corner singularities.[7] The smaller the θ_a, the slower is the transition to the corresponding limiting value. Obviously, the perfect-corner limit, being a matter of principle, is of minor practical importance.

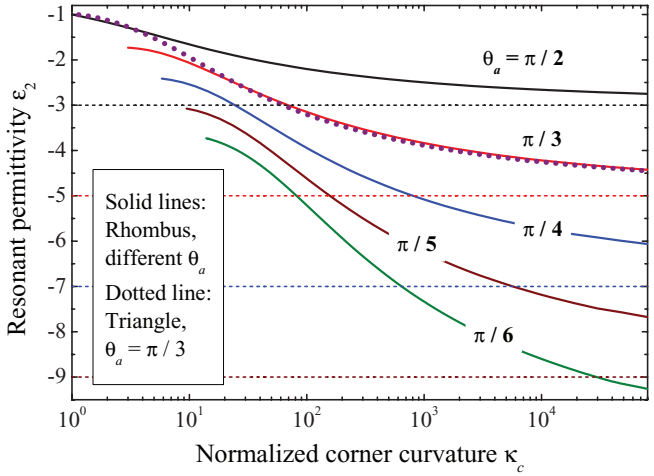

FIG. 4. (Color online) The lowest dipolar branch $\varepsilon_2(\kappa_c)$ for the smoothed rhombus with the apex angle $\theta_a = \pi/2,\pi/3,\pi/4,\pi/5$, and $\pi/6$ (solid lines) and a smoothed equilateral triangle with $\theta_a = \pi/3$ (dotted line). The horizontal dashed lines show the corresponding limiting values $\varepsilon(\infty) = 1 - 2\pi/\theta_a$.

A quick confluence of the dotted line (relevant to a circle → triangle transition) with the solid line corresponding to the rhombus with the same apex angle is remarkable. It shows explicitly that the lowest eigenvalues are strongly controlled by θ_a and κ_c for $\kappa_c \gg 1$, while the global shape of the particle is of minor importance.

B. Eigenfunctions: Charge localization

Here we consider the angular charge distributions for the most important eigenmodes. For simplicity, we restrict ourselves to the case of $4m$ symmetry ($\theta_a = \pi/2$).

Normalization of the eigenfunctions $\sigma_j(\varphi)$ and $\tau_j(\varphi)$ is generally a matter of convenience. The simplest choice is $\sigma_j^{\max} = \tau_j^{\max} = 1$. It allows one to see the most important tendency with increasing the corner curvature parameter κ_c: *localization of the surface charge* at the corners.

The solid lines in Fig. 5(a) show the eigenfunction $\sigma_2(\varphi)$ for the lowest dipolar branch calculated with the use of Eq. (11) for $\theta_a = \pi/2$ and $p = 4$, 8, and 64 ($\kappa_c \simeq 3.25$, 7.1, and 63, respectively).

All necessary symmetry properties (see Sec. IV) are fulfilled. Obviously, the surface-charge distribution exhibits sharp maximum and minimum at $\varphi = 0$ and π, respectively (at the charged corners), and turns to zero at $\varphi = \pi/2$ and $3\pi/2$ (at the uncharged corners). For $\kappa_c \simeq p/\sqrt{2} \gg 1$, the angular width of the peak is about $\kappa_c^{-1} = \rho_c/r_0 \ll 1$. Outside the close vicinities of the charged corners, the charge density $\sigma_2(\varphi)$ tends to zero for $\kappa_c \to \infty$. Remarkably, the function $\sigma_2(\varphi)$ changes its sign in between the charged and uncharged corners, and the corresponding zero points move towards the charged corners with increasing κ_c. This feature is not dictated by the symmetry properties or the charge neutrality.

The dotted lines in Fig. 5(a) are calculated using Eq. (13) for the same values of the corner curvature κ_c ($\simeq$2.8, 2.63, and 45.3) as the solid lines. For modest values of κ_c, there are some quantitative (but not qualitative) differences between two different representations of line L. When κ_c is increasing, these differences become negligible; see also Fig. 3. This situation is general for all results obtained for the $4m$ symmetry with the use of Eqs. (11) and (13). From now on, we will exhibit only the data obtained with Eq. (11).

The adjoint dipolar eigenfunction $\tau_2(\varphi)$, belonging to the same eigenvalue ε_2, is structurally similar to $\sigma_2(\varphi)$. In particular, it also shows maximum and minimum at the charged corners. However, localization of $\tau_2(\varphi)$ with increasing κ_c is much less pronounced.

The dipolar twin function $\sigma_{2'}(\varphi)$, possessing the eigenvalue $\varepsilon_{2'} = 1/\varepsilon_2$, is essentially different from $\sigma_2(\varphi)$ with respect to the localization type: The derivative $d\sigma_{2'}/d\varphi$ tends to infinity at the uncharged corners $\pi/2$ and $3\pi/2$ forming localized double layers; see Fig. 5(b). This feature is typical for the twin functions.

The higher-order dipolar eigenfunctions, $\sigma_5(\varphi)$, $\sigma_8(\varphi)$, etc., also experience localization at the corners with increasing κ_c; they possess a more complicated oscillatory structure far from the corners.

Figures 6(a) and 6(b) show the two lowest multipolar (quadrupolar) eigenfunctions $\sigma_1(\varphi)$ and $\sigma_3(\varphi)$ possessing the symmetries m_2^+ and m_1^+, respectively. Localization of the charge at all four corners with increasing κ_c is clearly seen. The charge neutrality in the case of Fig. 6(b) is ensured by the presence of nonlocalized charge; for Fig. 6(a), it is

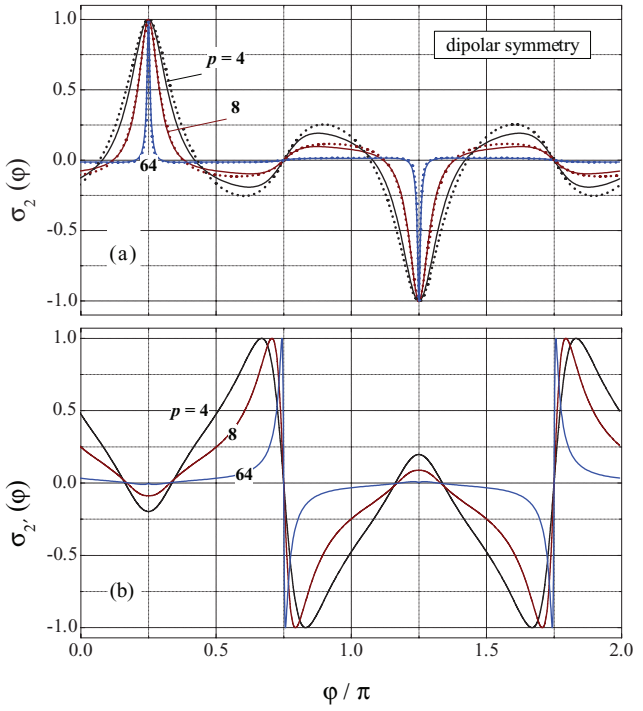

FIG. 5. (Color online) The case of square, $\theta_a = \pi/2$: The dipolar eigenfunctions (a) $\sigma_2(\varphi)$ and (b) $\sigma_{2'}(\varphi)$ calculated with Eq. (11) for $p = 4$, 8, and 64 (solid lines). The dotted lines in (a), given for comparison, refer to Eq. (13) and the same values of κ_c.

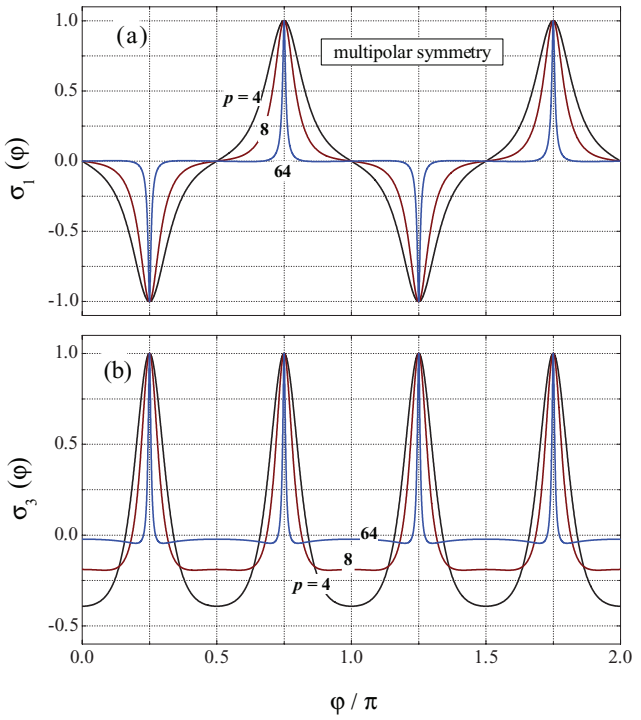

FIG. 6. (Color online) The lowest multipolar (quadrupolar) eigenfunctions (a) $\sigma_1(\varphi)$ and (b) $\sigma_3(\varphi)$ for $p = 4$, 8, and 64.

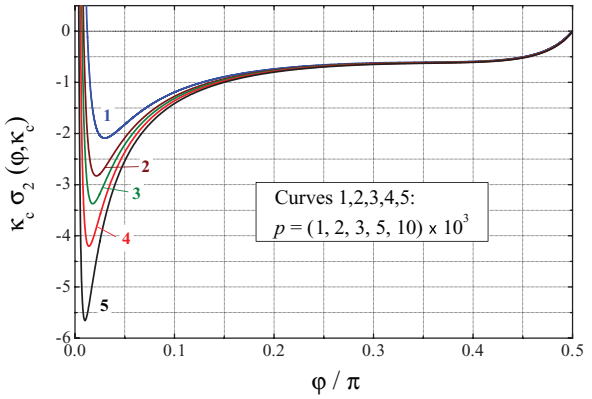

FIG. 7. (Color online) The lowest dipolar mode: The surface-charge distribution $\kappa_c\sigma_2(\varphi,\kappa_c)$ for several large values of the corner curvature κ_c within the angular interval $[0,\pi/2]$.

fulfilled automatically. The twin multipolar functions $\sigma_{1'}$ and $\sigma_{3'}$, possessing the symmetries m_2^- and m_1^-, show localized double-layer features, similar to that shown in Fig. 5(b), at all four corners for $\kappa_c \gg 1$.

As soon as the angular symmetry of the eigenfunctions is clear, their representation within the whole 2π interval of φ becomes excessive. It is sufficient to show the eigenfunctions within a quarter of the interval.

The data of Figs. 5 and 6 say almost nothing about the law of charge localization and about the relationship between the localized and nonlocalized charges. Furthermore, the used normalization of the eigenfunctions, $\sigma_j^{\max} = \tau_j^{\max} = 1$, implies that $\int_0^{2\pi} |\sigma_j(\varphi)|\, d\varphi \to 0$ for $\rho_c \to 0$, i.e., both the localized and nonlocalized charges tend to zero for a quarter of the square with increasing κ_c.

When dealing quantitatively with the charge localization, it is useful to consider the functions $\kappa_c\sigma_j(\varphi,\kappa_c)$. Their peak values are κ_c, while the angular width of the peaks is $\simeq\kappa_c^{-1}$. This means that the localized charge remains almost constant in κ_c, and one can expect that the localized part of $\kappa_c\sigma(\varphi,\kappa_c)$ near a charged corner can be represented by the Dirac δ function for $\kappa_c \to \infty$. On the other hand, the nonlocalized part becomes clearly accessible with this normalization.

Figure 7 shows in detail the negative tail of the charge distribution $\kappa_c\sigma_2(\varphi,\kappa_c)$ within a quarter of the angular interval, including the positively charge corner at $\varphi = 0$, for several large values of κ_c. For all curves, we are well outside the peak area, $\varphi \gg \kappa_c^{-1}$. Several features are worthy of attention:

(a) After a very sharp initial drop, the function $\kappa_c\sigma_2(\varphi,\kappa_c)$ changes its sign at a certain point $\varphi_0(\kappa_c)$, reaches a pronounced minimum at $\varphi_{\min}(\kappa_c)$, and then grows slowly up to the second zero point at the uncharged corner $\varphi = \pi/2$.

(b) Both characteristic angles, $\varphi_0(\kappa_c)$ and $\varphi_{\min}(\kappa_c)$, approach zero with increasing κ_c.

(c) The total negative (nonlocalized) charge exceeds 1 in the absolute value and grows slowly with κ_c. It is not small compared to the total positive charge.

(d) The minimum value of $\kappa_c\sigma_2(\varphi)$ also grows slowly with increasing κ_c.

(e) All shown curves practically coincide with each other far enough from the charged corner, showing a universal behavior within a broad interval of φ; this interval expands with increasing κ_c.

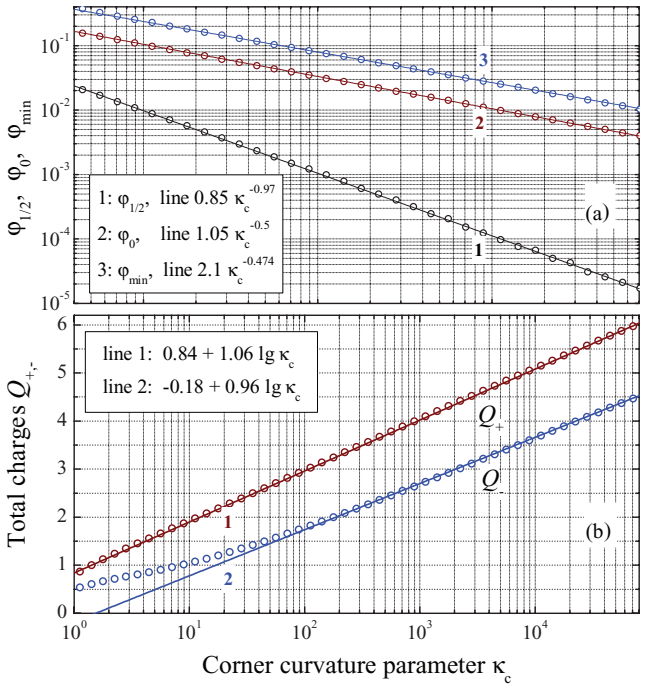

FIG. 8. (Color online) (a) The characteristic angles, $\varphi_{1/2}$, φ_0, and $\varphi_{\min}$ vs κ_c. (b) Dependence of the total charges $Q_\pm$ on κ_c. The circles in (a) and (b) are numerical data, while the solid straight lines are fitting functions; see the text.

Figure 8(a) exhibits the κ_c dependences of the characteristic angles—the half width of the peak $\varphi_{1/2}$, the zero point φ_0, and the point of minimum $\varphi_{\min}$—on a double logarithmic scale. The circles and straight solid lines refer to numerical data and power-fitting functions, respectively. Good agreement between the first and second is evident for sufficiently large corner curvatures. The characteristic angles tend to zero for $\kappa_c \to \infty$ by following different power laws. The decrease of $\varphi_{1/2}(\kappa_c)$ (line 1) is the fastest, while lines 2 and 3, representing φ_0 and $\varphi_{\min}$, are almost parallel to each other. We have found also that $[\kappa_c\sigma_2(\varphi,\kappa_c)]_{\min} \simeq -0.124\kappa_c^{0.43}$ for $\kappa_c \gtrsim 10$, i.e., the minimum value in Fig. 7 tends to $-\infty$ by following a power law. Thus, not only the peak of $\kappa_c\sigma_2(\varphi,\kappa_c)$, but also the growing negative tails are relevant to the charge localization at $\varphi = 0$.

Next we consider the total positive charge $Q_+ = 2\int_0^{\varphi_0} \sigma_2(\varphi)\, d\varphi/\rho_c$ localized near the corner $\varphi = 0$ and the absolute value of the total negative charge $Q_- = 2|\int_{\varphi_0}^{\pi/2} \kappa_c\sigma_2(\varphi)\, d\varphi|$ that is present on the right upper or right lower sides of the square; see also Fig. 2. The charge Q_- includes indeed both localized and nonlocalized contributions. The circles in Fig. 8(b) represent our numerical data for the dependences $Q_\pm(\kappa_c)$, while the solid lines 1 and 2 provide the corresponding fits. Both charges grow in κ_c, and they are comparable with each other in the whole range. At the same time, the growth is extremely slow—it is logarithmic for sufficiently large κ_c. The charge ratio Q_+/Q_-, which does not depend on the normalization of $\sigma_2(\varphi)$, remains larger than one in the whole shown range.

It is possible also to fit the function $\kappa_c\sigma_2(\varphi,\kappa_c)$ nearby the charged corner, namely, for $|\varphi| \lesssim \kappa_c^{-1}$. For $\kappa_c \gg 10$, the function $\kappa_c\,(1 + c\,\kappa_c^2\varphi^2)^{-0.7}$ with $c = c(\kappa_c) \approx 1$ approximates well the fall of $\sigma_2(\varphi)$ in the peak area within at least one order of magnitude. The peak profile is thus far from a Lorentzian one.

While the tendency to the charge localization and formation of singular charge structures for $\kappa_c \to \infty$ is clearly seen from our numerical calculations, there is no clear way to separate the singular and regular charge contributions. This issue will be discussed in Sec. VII.

With the known eigenfunctions $\sigma_j(\varphi) = \sigma_j[\mathbf{r}(\varphi)]\,l_\varphi$, we can calculate the modal dipole moments $\mathbf{d}_j = \int_0^{2\pi} \sigma_j(\varphi)\,\mathbf{r}(\varphi)\,d\varphi$. Obviously, they are nonzero only for the dipolar modes. It is clear from the above considerations that not only the localized but also nonlocalized modal charges contribute to $\mathbf{d}_j$ for large values of κ_c.

VI. RESONANT POLARIZABILITIES AND NEAR FIELDS

Here we restrict ourselves to the case of smoothed square. Because of the $4m$ symmetry, the polarizability is scalar, so that the light-induced dipole moment of the wire $\hat{\mathbf{d}} = \langle \mathbf{r}\hat{\sigma}(\mathbf{r})\rangle$, where $\hat{\sigma}(\mathbf{r})$ is the light-induced surface-charge density, is parallel to the external electric field vector $\mathbf{E}_0$. Correspondingly, the quantity $\alpha = |\hat{\mathbf{d}}|/|\mathbf{E}_0|$ calculated for an arbitrary orientation of the polarization vector $\mathbf{e}_0 = \mathbf{E}_0/|\mathbf{E}_0|$ gives the necessary polarizability.

When using the modal expansion (4), the light-induced dipole moment of the particle is given by $\hat{\mathbf{d}} = \sum c_j\mathbf{d}_j$, where the summation occurs only over the dipolar modes and c_j is given by Eq. (7). In accordance with this equation and our definitions, the vector $\hat{\mathbf{d}}$ does not depend on the normalization of the eigenfunctions σ_j and τ_j.

Since the lowest dipolar eigenvalues ε_j, with $j = 2,5,\ldots$, are well isolated from each other for $\rho_c^{-1} \gg 1$ (see Fig. 3), the corresponding plasmonic modes can be excited selectively and resonantly.

When calculating the resonant polarizability, it is necessary to keep in mind that a double degeneration occurs for the dipolar modes: The $\pi/2$-rotated functions $\sigma_j(\varphi + \pi/2)$ and $\tau_j(\varphi + \pi/2)$ belong to the same ε_j and are independent from the functions $\sigma_j(\varphi)$ and $\tau_j(\varphi)$, respectively. While the averages $\langle\tau_j\,\mathbf{n}\rangle$ and $\langle\sigma_j\,\mathbf{r}\rangle$ are parallel to the h diagonal, the same averages for the $\pi/2$-rotated functions are parallel to the v diagonal; see also Fig. 2. Missing this point leads to violation of the law $\hat{\mathbf{d}} \parallel \mathbf{E}_0$.

Setting $\varepsilon'_{\mathrm{M}}(\omega_j) = \varepsilon_j$ (the resonant condition for the jth mode) and $\mathbf{e}_0 = (1,0)$, we represent the polarizability in the form $\alpha_j = i\,G_j r_0^2/\varepsilon''_{\mathrm{M}}(\omega_j)$, where the dimensionless factor G_j is given by

$$G_j = \frac{(\varepsilon_j - 1)^2}{4\pi\, r_0^2}\,\frac{\langle\tau_j\,(\mathbf{e}_0\cdot\mathbf{n})\rangle\,\langle\sigma_j\,(\mathbf{e}_0\cdot\mathbf{r})\rangle}{\langle\sigma_j\tau_j\rangle}, \qquad (17)$$

and $\langle\cdot\rangle$ means again the integration along L. For a certain dipolar mode number j, this factor depends solely on the normalized corner curvature κ_c.

The presence of the imaginary unit in the expression for α_j means that a $\pi/2$ phase shift occurs between the temporal oscillations of the light electric field and those of the light-induced dipole moment; this feature is typical of the resonant phenomena. The resonant value of the polarizability grows indeed with decreasing loss factor $\varepsilon''_{\mathrm{M}}(\omega_j)$; this factor is controlled by material properties of the metal. Furthermore, the combination $s_j = 8\pi^2 r_0^2 G_j/\lambda_j\varepsilon''_{\mathrm{M}} \propto r_0^2/\lambda_j$ gives the resonant absorption cross section.

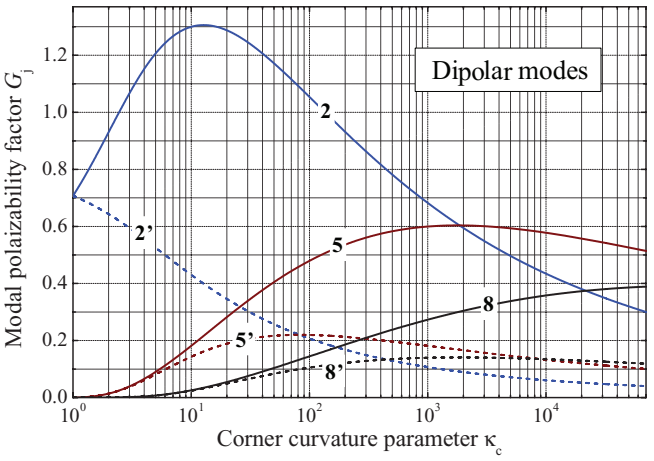

FIG. 9. (Color online) The dependence $G_j(\kappa_c)$ for the first three twin pairs of the dipolar modes: 2,2′, 5,5′, and 8,8′; see also Fig. 3.

The influence of the corner curvature on the resonant polarizabilities is given by the functions $G_j(\kappa_c)$. Figure 9 shows these functions for several first dipolar modes on a semilogarithmic scale. Within a wide range of κ_c, the biggest values of the G factor correspond to the lowest dipolar mode 2. The function $G_2(\kappa_c)$ possesses a broad maximum around $\kappa_c \approx 15$; near this maximum, $G_2 \gg G_{5,8}$. For $\kappa_c = 1$, we have $G_2 = 1/\sqrt{2}$; this corresponds to the limit of circular wire. For very large values of the corner curvature, $\kappa_c \gtrsim 10^3$, the higher dipolar modes 5 and 8 become competitive. The twin modes with $j = 2',5'$, and $8'$ possess relatively small G factors and, correspondingly, small polarizabilities.

When calculating the modal polarizability, we have found that the combination $\langle\tau_j\,(\mathbf{e}_0\cdot\mathbf{n})\rangle\,\langle\sigma_j\,(\mathbf{e}_0\cdot\mathbf{r})\rangle/\langle\sigma_j\tau_j\rangle$, entering Eq. (17), is the same for the dipolar twin modes 2 and 2′, 5 and 5′, etc. This expresses a certain hidden symmetry property. Because of this symmetry, the difference in polarizabilities α_j and in the G_j factors for the twin modes 2,2′, etc. is fully due to the difference in the factors $(\varepsilon_j - 1)^2$ in Eq. (17).

Next, we evaluate the resonant corner values of the light-induced charge density $\hat{\sigma}_j(0)$ for the horizontal light polarization vector, $\mathbf{e}_0 = (1,0)$. With our normalization $\sigma_j^{\max} = 1$, these values are given by $\hat{\sigma}_j(0) = \alpha_j|\mathbf{E}_0|/\langle\sigma_j\,(\mathbf{e}_0\cdot\mathbf{r})\rangle$. While the changes of α_j as a function of κ_c are modest (see Fig. 9), the factor $\langle\sigma_j\,(\mathbf{e}_0\cdot\mathbf{r})\rangle$ is roughly proportional to κ_c^{-1}. This is why $\hat{\sigma}_j(0) \propto \kappa_c$, i.e., a strong enhancement of the corner charge with increasing κ_c, takes place; see also below.

It is even more interesting to calculate the resonant light-induced field $\hat{\mathbf{E}}_j$ at the charged corner for $\mathbf{e}_0 = (1,0)$. This field has indeed only the normal (horizontal) component $\hat{E}_n^+(0)$ given by the two last terms in Eq. (5). While the first of these terms is given by the corner charge density $\hat{\sigma}(0)$, the second is integral—it depends on the distribution of the localized and nonlocalized charges along L. In the case of resonant

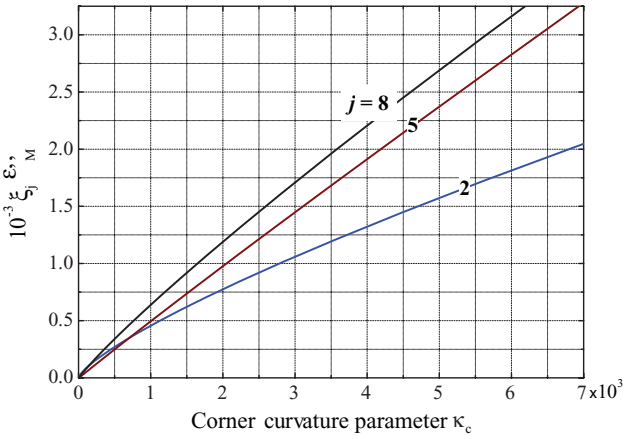

FIG. 10. (Color online) The product $\varepsilon''_{\rm M}\,\xi^c_j$ vs κ_c for the lowest dipolar modes $j = 2, 5, 8$. Note the scaling factor 10^3 along the axes.

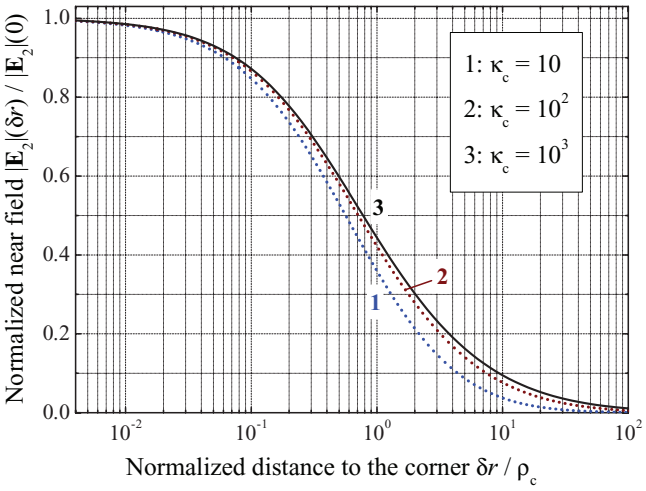

FIG. 11. (Color online) The normalized near field $|\mathbf{E}_2|(\delta r)/|\mathbf{E}_2|(0)$ vs the normalized distance to the corner along the h diagonal, $\delta r/\rho_c$, for the resonantly excited main dipolar mode ($j = 2$) and three values of the corner curvature parameter κ_c.

excitation of the mode j, the integral contribution is nothing else than $\Lambda_j\hat{\sigma}_j$, in accordance with Eq. (1). Thus, we have the following simple link between the resonant corner values of the light-induced field and charge: $|\hat{\mathbf{E}}_j(0)| = 4\pi\,\varepsilon_j\,|\hat{\sigma}_j(0)|/(\varepsilon_j - 1)$. Using the above relations for α_j and $\hat{\sigma}_j(0)$, we arrive at a simple relation for the resonant field-enhancement factor $\xi^c_j = |\hat{\mathbf{E}}_j(0)|/|\mathbf{E}_0|$ at the charged corners:

$$\xi^c_j = \frac{\varepsilon_j(\varepsilon_j - 1)}{\varepsilon''_{\rm M}}\,\frac{\langle\tau_j\,(\mathbf{e}_0\cdot\mathbf{n}\rangle}{\langle\sigma_j\,\tau_j\rangle}. \qquad (18)$$

The squared value of this factor gives the light intensity enhancement factor at the corner.

Figure 10 shows the dependence $\xi^c_j(\kappa_c)$ for the three lowest dipolar modes, $j = 2,5$, and 8. One sees that the field-enhancement factor grows approximately linearly with the corner curvature and increases by orders of magnitude for realistic values of κ_c. Remarkably, the lowest dipolar mode 2 possesses a relatively small enhancement factor compared to the higher dipolar modes 5 and 8. This contrasts with the properties of the modal polarizability; see Fig. 9. The behavior of $\hat{\sigma}_j(0)$ as functions of κ_c is similar to that presented in Fig. 10.

Lastly, we consider how fast the resonant field $\hat{\mathbf{E}}$ decreases with increasing normalized distance to the corner $\delta r/\rho_c = \kappa_c\delta r/r_0$. Figure 11 shows this dependence on a semilogarithmic scale for the main dipolar mode 2, the polarization vector $\mathbf{e}_0 = (1,0)$, and three values of κ_c. The field $\hat{\mathbf{E}}_2$ is directed here along the h diagonal, and δr is measured along this diagonal. With the chosen normalization, all three curves lie very close to each other, showing an almost universal behavior. It is evident that the function $|\mathbf{E}_2|(\delta r/\rho_c,\kappa_c)/|\mathbf{E}_2|(0)$ converges to a certain characteristic function of $\delta r/\rho_c$ with increasing κ_c. The half width of the function $|\mathbf{E}_2|(\delta r)/|\mathbf{E}_2|(0)$ is about the corner curvature radius ρ_c for $\kappa_c \gg 1$; this indicates again a strong charge localization at the corners. For $\delta r \gg \rho_c$, the decrease of $|\mathbf{E}_2|(\delta r)$ slows down because of the influence of the nonlocalized charge.

VII. DISCUSSION

Although we necessarily touched on classification of the plasmonic states, the main results of our study are about the universal behavior of plasmonic properties of metallic 2D nanoparticles with sharp corners and about the charge localization phenomenon. This involves several issues to discuss:

(a) Smoothing of corners is absolutely necessary to provide well-defined plasmonic eigenfrequencies and eigenfunctions. The apex angle θ_a and the normalized corner curvature $\kappa_c = r_0/\rho_c$ serve as the main control parameters for the lowest plasmonic eigenmodes: Different types of smoothing with the same values of θ_a and κ_c give essentially the same plasmonic properties for $\kappa_c \gg 1$, and the global shape of the particle is of minor importance.

(b) When the corner curvature increases, the lowest resonant values of the permittivity $\varepsilon_j(\kappa_p)$, dipolar and multipolar, decrease steadily and tend to the limiting value $\varepsilon(\infty) = 1 - 2\pi/\theta_a$. This value corresponds to a nonintegrable singularity of a single infinite corner.[7] Within the Drude model, the resonant frequencies ω_j tends to $\omega_p(\theta_a/2\pi)^{1/2}$. The smaller the θ_a, the stronger is the lowering of the resonant plasmonic frequency.

(c) For very large values of κ_c, the convergence of $\varepsilon_j(\kappa_c)$ to the limiting value of $\varepsilon(\infty)$ occurs extremely slowly: Even for unrealistically large values, $\kappa_c = (10^4$–$10^5)$, which bring us to a subatomic spatial scale, the values of ε_j are still not very close to $\varepsilon(\infty)$; see Figs. 3 and 4. Already in this sense, the limiting case $\rho_c \to \infty$ is practically unattainable, and the recent attempt to treat it heuristically[38] looks unjustified.

(d) Nevertheless, the impact of the increasing curvature is strong: First, it provides the charge localization on the scale of $\rho_c \ll r_0$. Second, it gives strong separation and red shifts of the plasmonic frequencies relevant to the localized dipolar modes. Altogether, it allows one to excite selectively the localized modes, leading to strong near-field enhancement of the light intensity.

(e) When looking at the structure of the eigenfunctions $\sigma_j(\varphi)$, it becomes evident (see, e.g., Figs. 5 and 7) that the charge localization cannot be approximated solely by the singular Dirac δ function for $\kappa_c \to \infty$. The angular derivatives of the δ function have to be involved as well. Furthermore, not

only the eigenfunctions $\sigma_j(\mathbf{r})$ but also the kernel $K(\mathbf{r},\mathbf{r}')$ of the basic integral equation becomes singular in this limit. This emphasizes the mathematical complexity of the transition to the perfect corner limit.

While the influence of the shape of metallic particles on the spectrum of plasmonic resonances, including the appearance of new red-shifted maxima, is known (see Refs. 27 and 29, and references therein), the knowledge of the plasmonic properties of nonspherical and nonelliptical nanoparticles remains fragmental and superficial. This is caused largely by vastness and uncertainty of the subject. The found universality of the plasmonic behavior for nanoparticles with sharp corners is the main difference with the previous studies.

A certain similarity of our physical picture with that of the wedge plasmons (WPs) propagating along sharp metallic corners[12,13] has to be mentioned. It concerns the importance of rounding of the corners for WPs. At the same time, the differences are evident: Nanolocalization of WPs is due to large values of the wave vectors; there is no transition to our case of nonpropagating localized plasmons. Furthermore, the WPs cannot be excited by laterally incident light, so that the observable characteristics and the areas of interest are different.

Consider now the upper limit of the corner curvature parameter $\kappa_c = r_0/\rho_c$. The value of $\rho_c^{\min}$, compatible with the notion of bulk optical permittivity, is $\sim$1 nm.[15,34] The size r_0 has to be considerably smaller than the light wavelength λ to avoid the retardation effects.[25] Most probably, the latter restriction is not severe—owing to the charge localization at the corners, there should not be strong modification of our theory for $r_0 \approx \lambda$. We can expect thus that $\kappa_c^{\max} = 10^2$–10^3 within the visible to near IR spectral range.

VIII. CONCLUSIONS

Plasmonic properties of 2D metallic nanoparticles with sharp corners show a universal behavior. The lowest values of the resonant optical permittivity ε_j, dipolar and multipolar, are controlled by the corner apex angle θ_a and the normalized corner curvature $\kappa_c \equiv r_0/\rho_c \gg 1$, while the global shape and smoothing details are of minor importance. The negative values of ε_j decrease with increasing κ_c and decreasing θ_a, causing strong red shifts of the plasmonic frequencies. The decrease of $\varepsilon_j(\kappa_c)$ is initially fast and then extremely slow so that the limiting value $\varepsilon(\infty) = 1 - 2\pi/\theta_a$ cannot be closely approached for $\kappa_c \lesssim 10^3$. The decrease of $\varepsilon_j(\kappa_c)$ is accompanied by localization of the corresponding eigenfunctions—the surface charge densities $\sigma_j(\varphi)$—near the corners at the angular scale of κ_c^{-1}. This localization is compatible with the properties of spatial symmetry. For realistic values of the corner curvature, $\kappa_c = 10^1$–10^3, the main dipolar resonances are well separated from each other. This allows one to excite them selectively, leading to a strong near-field enhancement of the light intensity at the corners.

ACKNOWLEDGMENTS

The work is supported by the Russian Academy of Sciences, Presidium Program 24 and BPS Program "Physics of new materials and structures."

[1] D. J. Bergman and M. I. Stockman, Phys. Rev. Lett. **90**, 027402 (2003).
[2] M. A. Noginov, G. Zhu, A. M. Belgrave, R. Bakker, V. M. Shalaev, E. E. Narimanov, S. Stout, E. Herz, T. Suteewong, and U. Wiesner, Nature (London) **460**, 1110 (2009).
[3] R. F. Oulton, V. J. Sorger, T. Zentgraf, R.-M. Ma, C. Gladden, L. Dai, G. Bartal, and X. Zhang, Nature **461**, 629 (2009).
[4] J. A. Schuller, E. S. Barnard, W. Cai, Y. C. Jun, J. S. White, and M. L. Brongersma, Nature Mater. **9**, 193 (2010).
[5] N. Liu, M. L. Tang, M. Hentschel, H. Giessen, and A. P. Alivisatos, Nature Mater. **10**, 631 (2011).
[6] L. D. Landau and E. M. Lifshits, *Electrodynamics of Continuous Media* (Pergamon, Oxford, 1984).
[7] J. Meixner, IEEE Trans. Antennas Propag. **AP-20**, 442 (1972).
[8] G. R. Hardley, J. Lightwave Technol. **20**, 1219 (2002).
[9] J. H. Hetherington and M. F. Thorpe, Proc. R. Soc. A **438**, 591 (1992).
[10] D. J. Bergman, J. Phys. C **12**, 4947 (1979).
[11] G. W. Milton, J. Math. Phys. **42**, 4873 (2001).
[12] L. Dobrzynski and A. A. Maradudin, Phys. Rev. B **6**, 3810 (1976).
[13] L. C. Davis, Phys. Rev. B **14**, 5523 (1972).
[14] H. Wallen, H. Kettunen, and A. Sihvola, Metamaterials **2**, 113 (2008).
[15] V. Klimov, *Nanoplasmonics* (Pan Stanford, Singapore, 2011).
[16] D. Kellogg, *Foundations of Potential Theory* (McGraw-Hill, New York, 1929).
[17] S. G. Mikhlin, *Mathematical Physics, an Advanced Course* (North-Holland, Amsterdam, 1970).
[18] J. Helsing and K.-M. Perfekt, Appl. Comput. Harmon. Anal. **34**, 445 (2013).
[19] R. Jin, Y. W. Cao, C. A. Mirkin, K. L. Kelly, G. C. Schatz, and J. G. Zheng, Science **294**, 1901 (2001).
[20] Y. Sun and Y. Xia, Science **298**, 2176 (2002).
[21] S. E. Habas, H. Lee, V. Radmilovic, G. A. Somorjai, and P. Yang, Nature Mater. **6**, 692 (2007).
[22] C. Hrelescu, T. K. Sau, A. L. Rogach, F. Jäckel, G. Laurent, L. Douillard, and F. Charra, Nano Lett. **11**, 402 (2011).
[23] V. Myroshnychenko, J. Nelayah, G. Adamo, N. Geuquet, J. Rodriguez-Fernandez, I. Pastoriza-Santos, K. F. MacDonald, L. Henrard, L. M. Liz-Marzan, N. I. Zheludev, M. Kociak, and F. J. Garcia de Abajo, Nano Lett. **12**, 4172 (2012).
[24] C. F. Bohren and D. R. Huffmann, *Absorption and Scattering of Light by Small Particles* (Wiley Interscience, New York, 1983).
[25] L. Novotny and B. Hecht, *Principles of Nano-Optics* (Cambridge University Press, New York, USA, 2006).
[26] R. Ruppin, Z. Phys. D **36**, 69 (1996).
[27] J. P. Kottmann and O. J. F. Martin, Appl. Phys. B **73**, 299 (2001).
[28] J. P. Kottmann, O. J. F. Martin, D. R. Smith, and S. Schultz, Phys. Rev. B **64**, 235402 (2001).

[29]K. L. Kelly, E. Coronado, L. L. Zhao, and G. C. Schatz, J. Phys. Chem. B **107**, 668 (2003).
[30]A. L. Gonzalez and C. Noguez, J. Comput. Theor. Nanoscience **4**, 231 (2007).
[31]N. Berkovitch, P. Ginzburg, and M. Orenstein, Nano Lett. **10**, 1405 (2010).
[32]F. Ouyang and M. Isaacson, Philos. Mag. B **60**, 481 (1989).
[33]I. D. Mayergoyz, D. R. Fredkin, and Z. Zhang, Phys. Rev. B **72**, 155412 (2005).
[34]M. I. Stockman, Opt. Express **19**, 22029 (2011).
[35]Note that the spectral method of Bergman (see Ref. 34, and references therein) also possesses similar features. However, it is less convenient for our purposes.
[36]L. D. Landau and E. M. Lifshits, *Quantum Mechanics* (Pergamon, Oxford, 1977), Chap. 12.
[37]E. Podivilov, B. Sturman, and M. Gorkunov, J. Opt. Soc. Am. B **29**, 3248 (2012).
[38]R. Vincent, J. I. Juaristi, and P. Apell, arXiv:1103.2086 [cond-mat.mtrl-sci] (2011).